Title

Scanning Tunneling Microscopy Study of the Structure and Interaction between Carbon Monoxide and Hydrogen on the Ru(0001) Surface

Journal

The Journal of Physical Chemistry B, 122(2)

ISSN

1520-6106

Authors

Lechner, Barbara AJ
Feng, Xiaofeng
Feibelman, Peter J
et al.

Publication Date

2018-01-18

DOI

10.1021/acs.jpcb.7b05657

Peer reviewed

THE JOURNAL OF PHYSICAL CHEMISTRY B

Article

pubs.acs.org/JPCB

Scanning Tunneling Microscopy Study of the Structure and Interaction between Carbon Monoxide and Hydrogen on the Ru(0001) Surface

Barbara A. J. Lechner,[†,⊥] Xiaofeng Feng,[†,#] Peter J. Feibelman,[‡] Jorge I. Cerdá,[§] and Miquel Salmeron*[,†]

[†]Materials Sciences Division, Lawrence Berkeley National Laboratory, Berkeley, California 94720, United States

[‡]Sandia National Laboratories, Albuquerque, New Mexico 87185, United States

[§]Instituto de Ciencia de Materiales de Madrid, ICMM-CSIC, Cantoblanco, 28049 Madrid, Spain

Supporting Information

ABSTRACT: We use scanning tunneling microscopy (STM) to investigate the spatial arrangement of carbon monoxide (CO) and hydrogen (H) coadsorbed on a model catalyst surface, Ru(0001). We find that at cryogenic temperatures, CO forms small triangular islands of up to 21 molecules with hydrogen segregated outside of the islands. Furthermore, whereas for small island sizes (3−6 CO molecules) the molecules adsorb at *hcp* sites, a registry shift toward *top* sites occurs for larger islands (10−21 CO molecules). To characterize the CO structures better and to help interpret the data, we carried out density functional theory (DFT) calculations of the structure and simulations of the STM images, which reveal a delicate interplay between the repulsions of the different species.

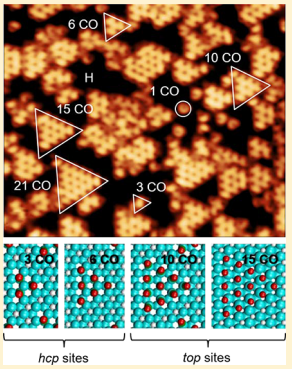

INTRODUCTION

Fischer−Tropsch (FT) synthesis produces liquid hydrocarbon fuels from syngas (a mixture of carbon monoxide, CO, and hydrogen, H_2), thus providing an important alternative to fuels derived from crude oil through the conversion of coal, natural gas, or, importantly, renewable resources such as biomass.[1,2] Efficient catalysts for this reaction are group VIII transition metals like Ru, Co, and Fe.[1,3] The first step in the process is CO dissociation and CH_x formation, which is then followed by chain length growth via CH_x−CH_x coupling reactions.[4] The detailed process of CO adsorption and bond breaking is still discussed extensively in the literature.[5−7] One major question regarding the initial step is whether CO dissociates into C and O directly upon adsorption on the catalyst surface or via the formation of CHO or COH intermediates with coadsorbed H atoms.[8−10] Theoretical evidence suggests that the latter process, that is, dissociation assisted by hydrogen, is the preferred one.[8,9,11] The short lifetime and low concentration of the intermediate species make their experimental identification difficult,[12,13] yet recent X-ray spectroscopy experiments have succeeded in identifying a CHO intermediate during CO hydrogenation.[14] Here, we study the coadsorption and interaction of CO and H at low temperatures to determine the structures formed and the potential role of H in CO dissociation. In particular, we investigate whether the reactants are intimately mixed on the surface. Segregation on a catalyst surface could impose kinetic limitations, although we should note that the behavior under reaction conditions may well be different from that observed at low pressures and temperatures.

Many experimental and theoretical studies have been performed to understand the interaction of CO and H on Ru surfaces. Early experimental work suggested strong segregation of the two species on Ru(0001), leading us to wonder where and how the reactants meet on the surface. For example, Peebles and co-workers performed temperature-programmed desorption (TPD) and X-ray photoelectron spectroscopy (XPS) and found evidence for long-range CO−H repulsive interactions resulting in different domains of CO and H on the surface.[15] Yet, even in the early studies of this system, some experiments hinted at a more complex behavior. Mak et al. deduced from their H surface diffusion studies a structure of small CO islands surrounded by a hydrogen exclusion area.[16] Theoretical calculations by van Santen et al. confirmed the repulsive CO−H lateral interaction and the formation of segregated islands rather than mixed structures.[17] Later, Riedmüller and co-workers reported the formation of CO islands when coadsorbed with H on Ru(0001). Using helium atom scattering (HAS), they deduced an average "magic" size of seven CO molecules per island.[18] Similarly, TPD experi-

Special Issue: Miquel B. Salmeron Festschrift

Received: June 9, 2017
Revised: July 22, 2017
Published: July 28, 2017

DOI: 10.1021/acs.jpcb.7b05657
J. Phys. Chem. B 2018, 122, 649−656

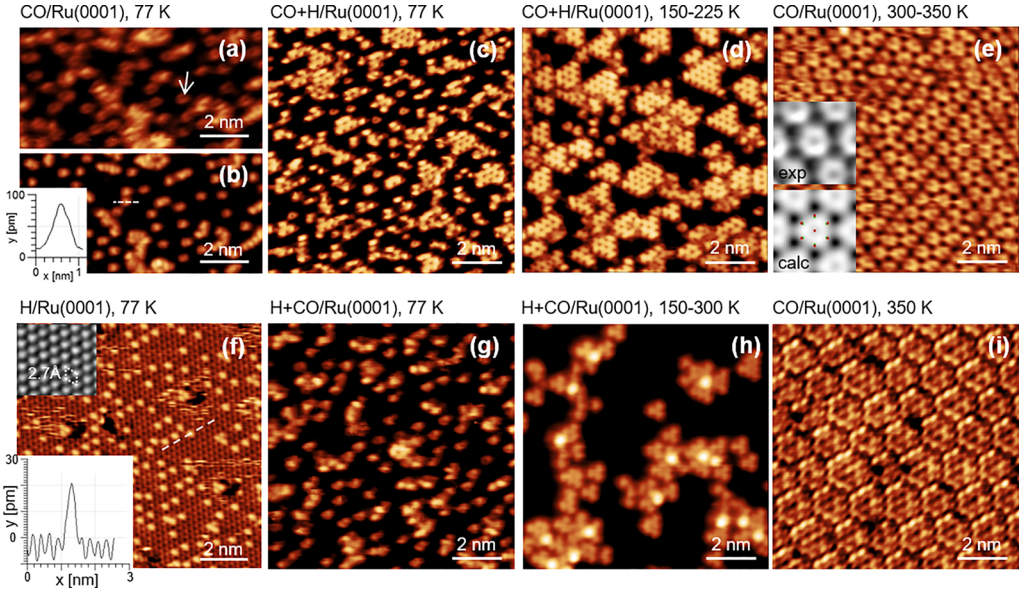

Figure 1. Evolution of the structures formed after adsorption of CO and H_2 on Ru(0001) and annealing to the specified temperature, followed by cooling back to 77 K. CO is imaged (a) as a protrusion with a depression in the center when using a Pt/Rh tip (cf. arrow) and (b) as a single protrusion of 70 pm height using a CO-terminated tip. (c) Coadsorbing CO and H_2 at 77 K results in a disordered arrangement of both species. (d) By annealing to temperatures in the range of 150−225 K we obtain dense triangular CO islands surrounded by H atoms (unresolved in the dark areas). The images correspond to a CO tip. (e) Upon annealing to 300−350 K, H_2 desorbs and CO forms a $(2\sqrt{3} \times 2\sqrt{3})R30°$-7CO structure, imaged with a metallic tip in this instance.[22] We confirm the structure assignment by comparing an experimental STM measurement (top inset) with STM image simulations (bottom inset; see also Figure S3a). (f) Hydrogen atoms, imaged as 8 pm deep depressions, form a (1 × 1) structure on Ru(0001), while H vacancies appear as 20 pm high protrusions (see the height profile in the bottom inset). Top inset: image of the bare Ru(0001). (g) Adsorbing CO onto a H-precovered surface at 77 K results in individual CO molecules and small islands, similar to the surface seen in (c). (h) Annealing to 150−300 K results once more in triangular CO islands analogous to (d), despite the lower total CO coverage on the surface (metallic tip). (i) Only after annealing to 350 K can we adsorb more CO to obtain a pure CO structure, here imaged with a CO-terminated tip.[22,28] Imaging parameters: (a) I_t = 23 pA, V_b = 103 mV; (b) I_t = 22 pA, V_b = 103 mV; (c) I_t = 21 pA, V_b = 26 mV; (d) I_t = 95 pA, V_b = 52 mV; (e) I_t = 28 pA, V_b = 28 mV; (f) I_t = 12 pA, V_b = 101 mV; (g) I_t = 247 pA, V_b = 311 mV; (h) I_t = 92 pA, V_b = 157 mV; (i) I_t = 17 pA, V_b = 31 mV.

ments using molecular beams to dose D_2 onto a CO-precovered surface showed the formation of complexes with a CO to deuterium (D) ratio of 1:1, involving attractive interactions between the two species on Ru(0001).[19] Another TPD study was reported for CO and H coadsorption on a Pt/Ru surface alloy, combined with infrared reflection absorption spectroscopy (IRAS), suggesting that the total coverage of adsorbed H and CO is higher than the sum of the saturation coverages of both molecules, again indicating attractive interactions between the two species.[20,21] These different findings indicate that the interaction potential between CO and H on a Ru surface is highly complex. It is therefore of paramount importance to investigate the coadsorption of CO and H on a model catalyst surface in real space—as opposed to the "averaging" techniques mentioned above—to determine the individual size and shape of the reported "magic" islands and/or complexes. We chose Ru(0001) as a model catalyst surface as it is known to act as an efficient catalyst for FT synthesis, all the while being a well-defined substrate.

Our results indicate that, although the two species repel, they do not segregate into large domains but do so instead at the nanometer scale to minimize the energy cost of CO−CO, CO−H, and H−H repulsion. Upon deposition at 77 K, largely disordered structures are observed, while subsequent annealing to temperatures between 150 and 225 K results in small triangular islands containing from 3 to 21 CO molecules in close proximity, stabilized by a surrounding (1 × 1)-H background. In agreement with previous TPD investigations of coadsorbed CO and H (D), we found that further annealing to 300−350 K results in hydrogen desorption[15,19] and CO rearranging into periodic structures of roughly hexagonal 7CO or 19CO units.[22]

METHODS

Our experiments were performed using a home-built low-temperature STM with an RHK SPM100 controller[23] operated in an ultrahigh vacuum (UHV) chamber with a base pressure of 7×10^{-11} mbar. A Ru(0001) single crystal was cleaned in a separate UHV chamber by argon ion sputtering (1 keV, 5×10^{-5} mbar of Ar) and annealing to 1670 K. To remove carbon impurities from the bulk, we cycled the sample between 770 and 1770 K in 5×10^{-8} mbar of O_2 repeatedly, followed by annealing to 1670 K in UHV to desorb any residual oxygen. Auger electron spectroscopy and STM confirmed that the resulting surface contained <1% of contaminants.

CO (99.9999%) and H_2 (99.9999%) were introduced through a dosing tube pointing at the sample held at 77 K inside of the cryostat of the STM. Reference experiments were performed at 5 K, where H_2 contamination is limited by the strong pumping effect of the liquid-helium-cooled cryostat (see the Supporting Information). To increase adsorbate mobility, we annealed the sample to temperatures between 150 and 350 K inside of the STM. The temperature was measured with a Lake Shore DT-470 silicon diode and PID-controlled using a Lake Shore Model 331 temperature controller by counter-heating with a resistive heater. All STM images were acquired in constant current mode at a sample temperature of 77 K using electrochemically etched Pt/Rh (80/20) tips. The tunneling

DOI: 10.1021/acs.jpcb.7b05657
J. Phys. Chem. B 2018, 122, 649−656

current and bias voltage are given in the respective figure captions. All images were obtained along approximately the same crystal direction, namely, with the tip scanning direction perpendicular to the close-packed Ru rows.

Theoretical calculations have been performed using the GREEN software package[24] for both atomic relaxations and STM image simulations. For the former, we employed the interface to the SIESTA[25] DFT pseudopotential formalism under the Generalized Gradient Approximation (GGA) for exchange−correlation.[26] A double zeta polarized (DZP) basis set was defined for all elements, with localized atomic orbitals after imposing a confinement energy of just 10 meV for C, O, and the first and second layer Ru atoms and 50 meV for the rest of the (bulk-like) Ru atoms. Real- and reciprocal-space integrations were performed with a resolution given by a mesh cutoff of 500 Ryd and k-meshes of around (18 × 18) relative to Ru(0001). Multiple two-dimensional unit cells and different CO and H coverages were considered (see the text below) with slabs typically comprising five Ru layers. STM images were simulated for most of the optimized structures following the prescription of ref 27, always assuming a Pt tip consisting of a sharp pyramid of 14 atoms on a semi-infinite Pt(100) substrate. Tunneling parameters were fixed to I_t = 1 nA and V_b = +0.1 V in all cases, although calculations under different tunneling conditions did not show any significant dependency of the image contrast on I_t or V_b, which only affected the overall corrugation.

RESULTS AND DISCUSSION

To identify the contrast features due to CO and H in the STM images, we first acquired images with each species adsorbed separately. In agreement with a previous publication,[22] we observe two different types of contrast for CO, depending on the tip termination. With a metallic tip (see Figure 1a), the molecules appear as a protrusion with a dark center, that is, "donut"-shaped. When several molecules are close to each other, the protrusions overlap, resulting in an even brighter protrusion in-between the molecules, often adopting complex shapes, which hinder direct determination of the number of molecules and/or their relative distances. Scanning the same area with a CO-terminated tip, on the other hand, enhances the resolution, as shown in Figure 1b. When this tip is located above an adsorbed molecule (which is oriented perpendicular to the surface), the orbitals of the two CO molecules overlap efficiently, resulting in a single round protrusion. The apparent height of CO on the Ru(0001) surface as imaged with a CO tip is also more uniform across the surface and largely independent of the proximity of other CO molecules. A cross section of a single molecule shows an apparent height of approximately 70 pm (inset to Figure 1b).

In contrast, H atoms appear as depressions on Ru(0001) (see Figure 1f).[29] Near monolayer (ML) saturation coverage, we observe a (1 × 1) arrangement of dark spots due to H atoms with interspersed bright features due to H vacancies, that is, sites not covered with H. The vacancy contrast is due to the high electron density of the exposed metal substrate. As a reference, an image of bare Ru(0001) with maxima corresponding to Ru atoms is shown in the top inset of Figure 1f. Because the dissociative adsorption of H_2 requires several neighboring vacancies, single-vacancy sites remain for a long time even in the presence of H_2 gas.[30] The apparent depth of the H depressions is approximately 8 pm, while theory predicts a value of just 2 pm for a metallic tip.

The various structures formed by coadsorbed CO and H on Ru(0001) at different temperatures and coverages are summarized in Figure 1. Specifically, we compare the evolution of surfaces obtained by dosing the two gases to produce high (Figure 1a−e) and low (Figure 1f−i) CO/H ratios. In the first case, we obtain a disordered mixed structure of individual molecules (bright spots) and groups of closely packed CO molecules forming small islands of approximately triangular shape up to 2 nm in size (Figure 1c). As we anneal the surface to temperatures between 150 and 225 K, the triangles (some of them truncated) become the majority features on the surface, as shown in Figure 1d. This indicates that CO prefers to coalesce into small clusters in the presence of H instead of spreading more evenly across the surface. Further annealing to 300−350 K leads to a restructuring where clusters of seven CO molecules are formed arranged in a $(2\sqrt{3} \times 2\sqrt{3})R30°$ phase (see Figure 1e), similar to that reported recently in ref 22. In agreement with that study, we conclude that the CO molecules in the clusters are bound to metal atoms in *on-top* positions. DFT confirms that a relaxed $(2\sqrt{3} \times 2\sqrt{3})R30°$-7CO structure is indeed stable, with the six outer CO molecules leaning away from each other to minimize repulsive interactions. The bottom inset to Figure 1e shows a simulated image based on the relaxed structure (with a metallic tip), which is in good correspondence with the experimental one. Regarding the possibility of additional H atoms being present between the molecules in the 7CO structure, our calculations show that the agreement with the experimental images worsens when H is added, indicating that it is a pure CO phase (see Figure S3).

Figure 1f shows a nearly fully H-covered surface forming a (1 × 1) structure. After dosing CO onto this surface with high H coverage, it adsorbs, forming a disordered array of individual molecules occupying former H-vacancy sites and small islands (see Figure 1g). After annealing to temperatures between 150 and 300 K, triangular CO islands are formed, separated by large areas of low contrast, as shown in Figure 1h. These areas are filled with H atoms, which are difficult to observe because of the large (factor 10) difference in CO and H corrugation. Only by enhancing the contrast by plotting the image in derivative mode can the (1 × 1)-H structure be seen, as shown in Figure 2d,e in the areas marked by dashed rectangles in the bottom part of Figure 2b,c, respectively. A slight distortion of the (1 × 1) pattern close to the edges of the CO islands indicates that it corresponds to the adsorbed H lattice and not the Ru(0001) lattice. Literature reports[22] and our own reference experiments show that pure CO does not form compact isolated islands on Ru(0001). In agreement, our DFT calculations in the absence of H also favor a sparse arrangement of CO molecules rather than clusters, owing to their intermolecular repulsion (see Figure S2). To further confirm this, we dosed additional H_2 onto a surface like that in Figure 1h. The resulting images showed a similar distribution of dense CO islands separated by similar large areas without CO (see Figure S1).

We now look at the structures of compact CO islands stabilized by surrounding H in more detail to improve our understanding of the energetics that drives their formation. We first notice that the triangular islands in Figure 1d are all oriented in the same direction, with one vertex pointing toward the left. Images from larger areas, such as those in Figure 2a (see also Figure S5), reveal that the island orientation is always the same within one terrace but changes, alternating between left and right orientation from one terrace to a neighboring one

DOI: 10.1021/acs.jpcb.7b05657
J. Phys. Chem. B 2018, 122, 649−656

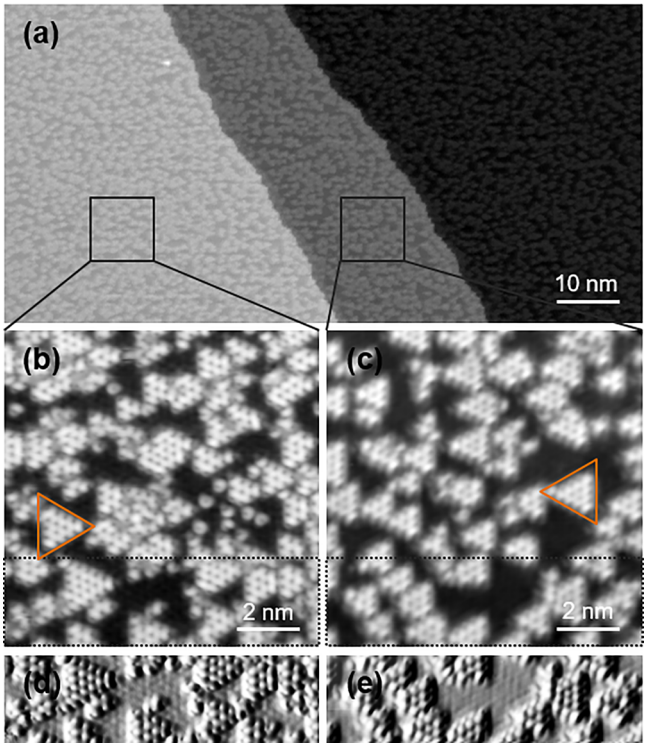

Figure 2. Alternating orientation of triangular CO islands in neighboring terraces. (a) Large-scale view, showing an even distribution of islands on three terraces of the Ru(0001) crystal. (b,c) Detailed images from neighboring terraces showing that the orientation of the islands alternates between orientations rotated by 120°, appearing as right- and left-pointing triangles, respectively. (d,e) Derivative images of the sections marked by dashed rectangles in (b) and (c), respectively, showing the hydrogen lattice between the CO islands. Imaging parameters: (a) I_t = 112 pA, V_b = 65 mV; (b) I_t = 80 pA, V_b = 65 mV; (c) I_t = 42 pA, V_b = 65 mV.

separated by a monatomic step. This is evident in the close-up images in Figure 2b,c. The 120° difference in orientation of the CO islands in neighboring terraces (also found previously for other adsorbates on close-packed metallic surfaces[31,32]) signals the relevance of the interactions with the second metal layer as its presence reduces the 6-fold symmetry to 3-fold.

Figure 3 shows close-up images of CO triangular islands of increasing size. The images, corresponding to a metallic tip, show the characteristic donut shape of single CO molecules (Figure 3a). Consequently, we identify the single bright protrusion surrounded by three depressions in Figure 3b as a 3CO cluster. A 6CO island appears as 3 bright lobes surrounded by 6 depressions (Figure 3c), a 10CO island shows six bright lobes surrounded by 10 depressions (Figure 3d), and so on (Figure 3e,f). Overall, we observe islands composed of up to 21 CO molecules. Measuring the distance between the centers of neighboring CO molecules, we find that the apparent CO−CO distance decreases with island size, from 4.3 Å in trimers to 3.2 Å in the 21CO island. These distances are all larger than, but successively approaching, the nearest-neighbor Ru−Ru distance of a_{Ru} = 2.7 Å, indicating a very dense CO structure and stressing the considerable lateral pressure exerted by the surrounding H-covered areas. In comparison, on Pt(111), a dense $(\sqrt{19}) \times \sqrt{19})$R23.4°-13CO structure with a CO−CO distance of 3.3 Å was found as a saturation coverage at 170 K and also under 1 bar of CO pressure at room temperature.[33,34] Nevertheless, none of the distances in the figure are commensurate with the Ru(0001) lattice, suggesting that not all CO molecules adsorb at the highest-symmetry position or that some are tilted to minimize repulsion, as confirmed by our DFT calculations. Another striking feature is that the smaller 3CO triangles appear to have an inverted orientation with respect to the larger ones. As will be discussed below, this is a key hint for determining the structure of the islands.

We performed DFT calculations to understand the energetics leading to CO island formation. Focusing first on 3CO and 6CO triangles within a $(2\sqrt{3} \times 2\sqrt{3})$R30° and a $(\sqrt{13} \times \sqrt{13})$R13.9° unit cell, respectively, we considered all possible triangular arrangements assuming an initial configuration where all CO molecules occupy the same site (*hcp*, *fcc*, or *top*) with overall *p*3*m* symmetry. The choice of these unit cells, corresponding to CO coverages of Θ_{CO} = 0.25 and 0.46 ML, respectively, represents a compromise between the locally ordered triangular phases obtained in some experiments (see Figure S4) and the images shown in Figure 3 where the islands are sparsely distributed. Because each triangle may be oriented pointing to the right or to the left depending on the site where its epicenter is placed, there are a total of six configurations per CO coverage (we denote each by the convention NCO_x^y, where N gives the number of CO molecules in the island, x refers to their adsorption sites, and y is the triangle's epicenter registry). In all cases, and to account for the H-covered inter-island areas, we occupied the empty *fcc* sites by hydrogen atoms except those lying near the CO molecules (i.e., those *fcc* sites with a surface-projected distance to any CO site smaller than the Ru lattice parameter, a_{Ru}). Unfortunately, these assumptions lead to unit cell models with different H coverages, namely, 5H for $3CO_{top}^{fcc}$ and $3CO_{hcp}^{fcc}$, 6H for $3CO_{top}^{hcp}$ and $3CO_{hcp}^{top}$, 9H for $3CO_{fcc}^{top}$ and $3CO_{fcc}^{hcp}$, 1H for $6CO_{top}^{hcp}$ and $6CO_{hcp}^{top}$, 3H for $6CO_{top}^{fcc}$ and $6CO_{hcp}^{fcc}$, and, finally, 7H for $6CO_{fcc}^{top}$ and $6CO_{fcc}^{hcp}$. Therefore, the standard total energy comparison between the triangular configurations for a given island size cannot be systematically applied here to discriminate the most favorable one; in fact, because for each H coverage there are two possible NCO_x^y configurations, we can only rule out the less stable within each pair. To circumvent this drawback, we additionally performed STM simulations for each model and relied on their comparison with experimental images. Both the relaxed geometries and their simulated STM images are displayed in Figures 4 and 5. It turns out that the only arrangements that satisfy the above stability criteria, match the experimental images, and, at the same time, satisfy the triangle's orientation inversion (the key hint mentioned above) are the $3CO_{hcp}^{top}$ + 6H and the $6CO_{hcp}^{fcc}$ + 3H configurations, corresponding to coverages for each species of $\Theta_{CO/H}$ = 0.25/0.50 and 0.46/0.24, respectively. Thus, all molecules in the 3CO and 6CO islands remain close to *hcp* sites, which, according to our total energy calculations, is the most favorable situation for an isolated CO, closely followed by the *top* site. In both island structures, CO−CO repulsion induces lateral shifts of the C atoms of around 0.2 Å and tilting of the molecules by 4−6°, which increases the O−O distances to 3.2−3.3 Å. In the 6CO triangles, however, the three corner C atoms experience even larger shifts of 0.6 Å to end up close to *bridge* sites and show hardly any tilting. Also notice that, apart from the NCO_{fcc}^y cases, which hold the largest H coverage in the inter-island regions but with all H atoms at unfavorable a_{Ru} in-plane distances to a CO, the NCO_{hcp}^{fcc} structures are the next ones to maximize the number of available *fcc* sites for the H atoms (i.e., provide a

DOI: 10.1021/acs.jpcb.7b05657
J. Phys. Chem. B 2018, 122, 649−656

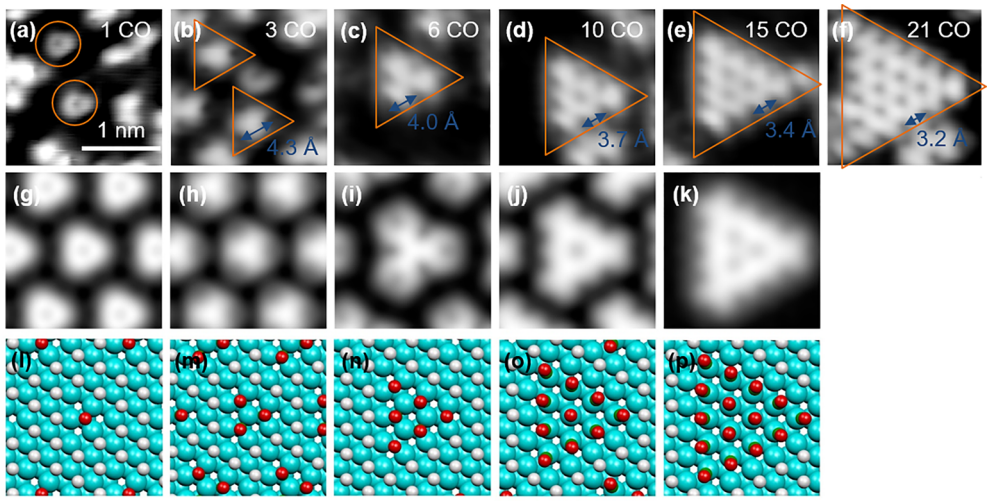

Figure 3. STM images (top), calculated images (middle), and structural models (bottom) of CO islands of increasing size. (a) A single CO molecule (marked by circles) appears as a donut shape in our STM images with a depression at its center. (b–f) In islands with several CO molecules (marked by triangles), the electron density in the donut shapes overlaps, resulting in brighter contrast at the center of the triangle formed by three neighboring CO molecules. Measuring the distance between the dark spots, that is, the O–O distance, we find that islands with 3, 6, 10, 15, and 21 CO molecules become increasingly denser, with CO–CO distances decreasing from 4.3 to 3.2 Å. All images have the same scale as that in (a). (g–k) STM image simulations of 1, 3, 6, 10, and 15 CO molecules surrounded by (1 × 1)-H show excellent agreement with experiment. (l–p) Optimized structures from DFT calculations for CO (C atoms in green, O in red) and H (white) on Ru (cyan) show a registry shift in the CO adsorption sites from *hcp* (1, 3, and 6CO units) to *top* (10CO and 15CO islands). The unit cells employed in the DFT relaxations and STM simulations are: (g,l) and (h,m) $(2\sqrt{3} \times 2\sqrt{3})$R30°; (i,n) and (j,o) $(3\sqrt{3} \times 3\sqrt{3})$R30°; and (k,p) p(9 × 9). Note that for the sake of comparison the 6CO triangular island in (i,n) has been computed under a unit cell larger than that employed for the same model in Figure 5b; however, the relaxed structure is essentially the same for both cells. Imaging parameters: (a) I_t = 112 pA, V_b = 65 mV; (b,f) I_t = 80 pA, V_b = 65 mV; (c,d,e) I_t = 42 pA, V_b = 65 mV.

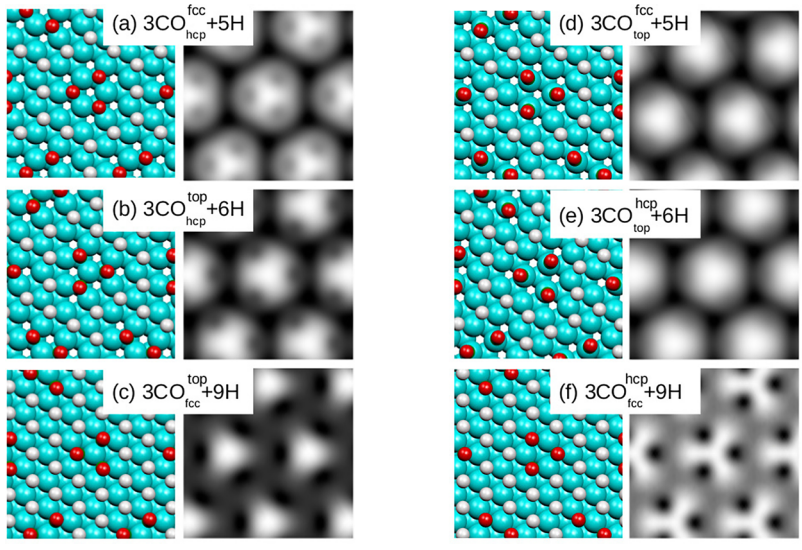

Figure 4. Top view (left panels) of the relaxed geometries and STM simulations (right panels) for several Ru(0001)-$(2\sqrt{3} \times 2\sqrt{3})$R30°-3CO + *n*H model structures, namely, (a) $3CO^{fcc}_{hcp}$ + 5H, (b) $3CO^{top}_{hcp}$ + 6H, (c) $3CO^{top}_{fcc}$ + 9H, (d) $3CO^{fcc}_{top}$ + 5H, (e) $3CO^{hcp}_{top}$ + 6H, and (f) $3CO^{hcp}_{fcc}$ + 9H (see the main text for the nomenclature employed to denote the structures). Within each row, the two structures share the same H coverage, with the more stable of the two displayed in the left column.

larger CO + H total coverage). Furthermore, as shown in Figure S7, where $6CO_{hcp}$ islands of different shapes and orientations are illustrated, always surrounded by a H-(1 × 1) background, our derived NCO^{fcc}_{hcp} structure maximizes the H coverage, therefore explaining the preference of CO to adopt well-oriented triangular shapes.

To confirm that CO and H are segregated, we recalculated all $3CO^{y}_{x}$ structures after placing one additional H atom at the triangle's epicenter. However, as shown in Figure S6, none of the simulated images provides a good match to experiment, and therefore, these structures may be ruled out. In fact, in most of these relaxations, the CO molecules shift from their initial three-fold sites away from the H owing to the repulsion that they experience, while for the CO^{y}_{top} configurations, the shift is not so large but the molecules end up with large tilt angles (pointing away from the H). This result indicates complete CO and H segregation on the Ru(0001) surface already taking place at the nanometer scale, in accordance with previous theoretical

DOI: 10.1021/acs.jpcb.7b05657
J. Phys. Chem. B 2018, 122, 649–656

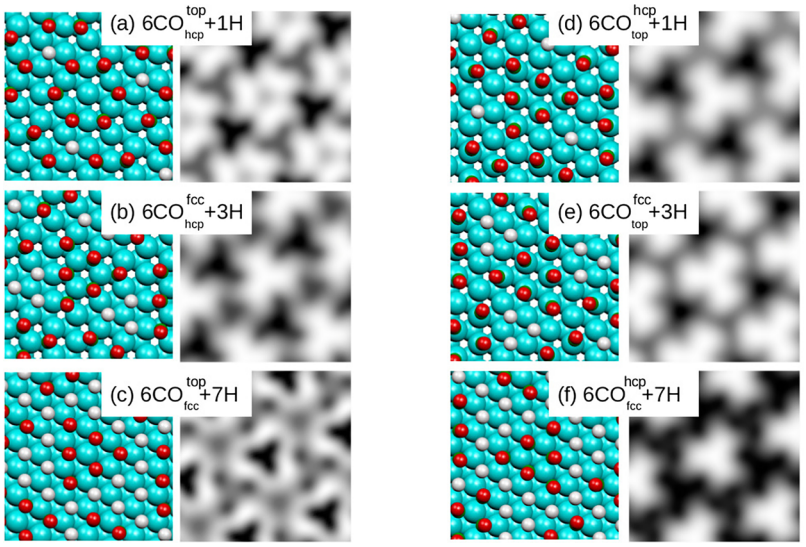

Figure 5. Top view (left panels) of the relaxed geometries and STM simulations (right panels) for several Ru(0001)-($\sqrt{13} \times \sqrt{13}$)R13.9°-6CO + *n*H model structures, namely, (a) $6CO^{top}_{hcp}$ + 1H, (b) $6CO^{fcc}_{hcp}$ + 3H, (c) $6CO^{top}_{fcc}$ + 7H, (d) $6CO^{hcp}_{top}$ + 1H, (e) $6CO^{fcc}_{top}$ + 3H, and (f) $6CO^{hcp}_{fcc}$ + 7H (see the main text for the nomenclature employed to denote the structures). Within each row, the two structures share the same H coverage, with the more stable of the two displayed in the left column.

studies.[17] We ascribe the absence of local CO−H mixing to the high coverage on the surface ($\Theta_{CO} + \Theta_H > 0.7$). For instance, a mixed (2 × 2)-CO_{hcp} + H_{fcc} structure with CO−H nearest-neighbor distances of $4/3a_{Ru}$ presents high stability, but its total coverage is only 0.5.

Last, we consider the larger 10CO and 15CO islands (the 21CO case is beyond our computational capabilities). From the above analysis, we would expect the molecules to remain at or close to *hcp* sites, and because their orientation is the same as that in the 6CO islands, the anticipated configurations should correspond to $10CO^{hcp}_{hcp}$ and $15CO^{top}_{hcp}$. However, the STM simulation for the former island employing a ($3\sqrt{3} \times 3\sqrt{3}$)R30° unit cell, shown in Figure 6, shows clear deviations with respect to the experimental one because of the large displacement of the corner atoms, which prefer to shift to the nearby (available) *fcc* sites. Accordingly, we have relaxed the other two possible configurations that preserve the island orientation, namely, $10CO^{top}_{top}$ and $10CO^{fcc}_{fcc}$, to find that only the former reproduces correctly the experimental STM image in Figure 3d (see Figure 6). Hence, the CO molecules in the islands undergo an unusual registry shift from *hcp* to *top* sites upon increasing their size from 6 to 10 molecules. Furthermore, this *top* configuration seems to be preserved in the largest islands because a $15CO^{fcc}_{top}$ island model (calculated within a Ru(0001)-(9 × 9) unit cell with up to 56 H_{fcc} atoms) again yields good agreement with the experiment, as can be seen in Figure 3e,k. Details of the 10CO island relaxed geometry reveal that, again, the carbon atoms undergo considerable lateral shifts (0.4−0.5 Å) away from the *top* registry while the molecules bend by as much as 25° (the central atom, however, does not shift and remains untilted owing to symmetry constraints). Such a large difference in the tilt angle between the 3/6CO and 10/15CO islands is most probably the reason for the change in molecular registry. In the former cases, *hcp* adsorption hinders large CO bending but, as the island size increases, so does the total CO−CO repulsion energy and the nanostructure stabilizes (i.e., reduces this repulsion energy) by shifting the molecules close to the *top* sites where CO tilting is less unfavorable in terms of the CO−Ru interaction energy. Thus, for islands of

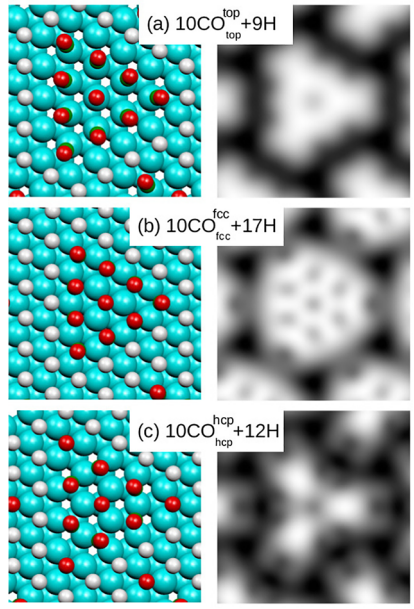

Figure 6. Top view (left panels) of the relaxed geometries and STM simulations (right panels) of possible high-symmetry model structures for a 10CO triangular island surrounded by (1 × 1)-H_{fcc} areas, namely, (a) $10CO^{top}_{top}$ + 9H, (b) $10CO^{fcc}_{fcc}$ + 17H, and (c) $10CO^{hcp}_{hcp}$ + 12H. A Ru(0001)-($3\sqrt{3} \times 3\sqrt{3}$)R30° unit cell has been employed in these calculations. See the main text for the nomenclature employed to denote the structures.

≥10 CO molecules, their structure is determined by minimizing the CO−CO repulsion as well as maximizing the H coverage (see also Figure S8).

A final comment on the thermal stability of the CO islands is important here. By repeating the STM measurements at higher temperatures, we find that the island structure is stable even after diffusion sets in. At 170 K, the islands diffuse on terraces between consecutively recorded STM images (65 s/frame) and change their shape, yet the overall triangular character is still clearly visible (see Figure S9). Furthermore, the alternating

DOI: 10.1021/acs.jpcb.7b05657
J. Phys. Chem. B 2018, 122, 649−656

orientation of the triangles on neighboring monatomic steps is maintained. Heating to 180 K, the diffusion becomes much more pronounced and the island shape less well-defined (see Movie S1). From a temperature of approximately 200 K, the molecules move too fast to be captured with the image frame rates available in our experiment. The observation of triangular islands at temperatures where diffusion occurs confirms that our measurements are not observations of kinetically trapped states.

CONCLUSIONS

In conclusion, we have shown that CO and H, when coadsorbed on Ru(0001), locally segregate at temperatures up to 225 K, forming small islands comprised of up to 21 molecules compressed into quasi-(1 × 1) arrangements surrounded by H atoms. Our results indicate that the CO−H repulsion is strong and prevents any local CO−H mixing. The CO−CO repulsion shows complex behavior where the molecules, packed in quasi-(1 × 1) arrangements, shift their binding sites from *hcp* in small islands to *top* sites in the larger islands. Presumably, the *top* configuration provides the CO molecules at the edge of the islands the possibility to tilt and mitigate the repulsive stress in the island. Under various conditions, CO adsorption on *top*, *hollow*, *bridge*, and non-high-symmetry adsorption sites have been reported on Ru(0001).[22,35−37] The observation of the simultaneous occupation of different adsorption sites on the same sample, as in the present experiments, can thus shed light on discrepancies in the literature. The influence of other effects on the adsorption site, such as vibrational dynamics, will be investigated in a future paper.

Furthermore, the close proximity of the adsorbate species to each other (with distances varying between 3.0 and 3.7 Å) could explain the high catalytic activity of Ru surfaces in the Fischer-Tropsch process, where CO and H react to form hydrocarbon chains. Although in the context of the FT synthesis our experimental conditions are still far from the real ones, we always obtain segregated CO and H phases, even within local phases of just a few nm in size, so that any CO−H reactions can only be induced at the edges of the islands.

ASSOCIATED CONTENT

Supporting Information

The Supporting Information is available free of charge on the ACS Publications website at DOI: 10.1021/acs.jpcb.7b05657.

Evidence for the presence of hydrogen in the triangular island phase; periodic arrays of islands; structure of the islands; and thermal stability of the islands (PDF)

STM movie of the thermal stability of the islands (AVI)

AUTHOR INFORMATION

Corresponding Author

*E-mail: mbsalmeron@lbl.gov.

ORCID

Barbara A. J. Lechner: 0000-0001-9974-1738

Miquel Salmeron: 0000-0002-2887-8128

Present Addresses

[⊥]B.A.J.L.: Chair of Physical Chemistry, Department of Chemistry, Technical University of Munich, Lichtenbergstr. 4, 85748 Garching, Germany.

[#]X.F.: Department of Physics, University of Central Florida, Orlando, FL 32816, U.S.A.

Notes

The authors declare no competing financial interest.

ACKNOWLEDGMENTS

This work was supported by the Office of Basic Energy Sciences, Division of Materials Sciences and Engineering of the U.S. DOE, under Contract No. DE-AC02-05CH11231. The theoretical calculations by J.I.C. were supported by the Spanish Ministry of Economy and Competitiveness through Grant No. MAT2015-66888-C3-1R, MINECO/FEDE. Calculations by P.J.F. were funded by Sandia National Laboratories, a multimission laboratory managed and operated by National Technology and Engineering Solutions of Sandia LLC, a wholly owned subsidiary of Honeywell International Inc. for the U.S. Department of Energy's National Nuclear Security Administration under Contract DE-NA0003525.

REFERENCES

(1) Van Santen, R. A.; Markvoort, A. J.; Filot, I. A. W.; Ghouri, M. M.; Hensen, E. J. M. Mechanism and Microkinetics of the Fischer−Tropsch Reaction. *Phys. Chem. Chem. Phys.* **2013**, *15* (40), 17038.

(2) Okabe, K.; Murata, K.; Nakanishi, M.; Ogi, T.; Nurunnabi, M.; Liu, Y. Fischer−Tropsch Synthesis over Ru Catalysts by Using Syngas Derived from Woody Biomass. *Catal. Lett.* **2009**, *128*, 171−176.

(3) Van der Laan, G. P.; Beenackers, A. A. C. M. Kinetics and Selectivity of the Fischer−Tropsch Synthesis: A Literature Review. *Catal. Rev.: Sci. Eng.* **1999**, *41*, 255−318.

(4) Shetty, S.; Van Santen, R. A. CO Dissociation on Ru and Co Surfaces: The Initial Step in the Fischer−Tropsch Synthesis. *Catal. Today* **2011**, *171* (1), 168−173.

(5) Rofer-DePoorter, C. K. A Comprehensive Mechanism for the Fischer−Tropsch Synthesis. *Chem. Rev.* **1981**, *81* (5), 447−474.

(6) Tuxen, A.; Carenco, S.; Chintapalli, M.; Chuang, C. H.; Escudero, C.; Pach, E.; Jiang, P.; Borondics, F.; Beberwyck, B.; Alivisatos, A. P.; et al. Size-Dependent Dissociation of Carbon Monoxide on Cobalt Nanoparticles. *J. Am. Chem. Soc.* **2013**, *135* (6), 2273−2278.

(7) Ojeda, M.; Nabar, R.; Nilekar, A. U.; Ishikawa, A.; Mavrikakis, M.; Iglesia, E. CO Activation Pathways and the Mechanism of Fischer−Tropsch Synthesis. *J. Catal.* **2010**, *272* (2), 287−297.

(8) Shetty, S.; Jansen, A. P. J.; Van Santen, R. A. Direct versus Hydrogen-Assisted CO Dissociation. *J. Am. Chem. Soc.* **2009**, *131* (36), 12874−12875.

(9) Ciobica, I. M.; Van Santen, R. A. Carbon Monoxide Dissociation on Planar and Stepped Ru(0001) Surfaces. *J. Phys. Chem. B* **2003**, *107*, 3808−3812.

(10) Tison, Y.; Nielsen, K.; Mowbray, D. J.; Bech, L.; Holse, C.; Calle-Vallejo, F.; Andersen, K.; Mortensen, J. J.; Jacobsen, K. W.; Nielsen, J. H. Scanning Tunneling Microscopy Evidence for the Dissociation of Carbon Monoxide on Ruthenium Steps. *J. Phys. Chem. C* **2012**, *116* (27), 14350−14359.

(11) Alfonso, D. R. Further Theoretical Evidence for Hydrogen-Assisted CO Dissociation on Ru(0001). *J. Phys. Chem. C* **2013**, *117*, 20562.

(12) Mitchell, W. J.; Xie, J.; Jachimowski, T. A.; Weinberg, W. H. Carbon Monoxide Hydrogenation on the Ru(001) Surface at Low Temperature Using Gas-Phase Atomic Hydrogen: Spectroscopic Evidence for the Carbonyl Insertion Mechanism on a Transition Metal Surface. *J. Am. Chem. Soc.* **1995**, *117*, 2606.

(13) Morgan, G. A.; Sorescu, D. C.; Zubkov, T.; Yates, J. T. The Formation and Stability of Adsorbed Formyl as a Possible Intermediate in Fischer−Tropsch Chemistry on Ruthenium. *J. Phys. Chem. B* **2004**, *108* (11), 3614−3624.

(14) LaRue, J.; Krejčí, O.; Yu, L.; Beye, M.; Ng, M. L.; Öberg, H.; Xin, H.; Mercurio, G.; Moeller, S.; Turner, J. J.; et al. Real-Time

Elucidation of Catalytic Pathways in CO Hydrogenation on Ru. *J. Phys. Chem. Lett.* **2017**, *8* (16), 3820−3825.
(15) Peebles, D. E.; Schreifels, J. A.; White, J. M. The Interaction of Coadsorbed Hydrogen and Carbon Monoxide on Ru(001). *Surf. Sci.* **1982**, *116*, 117−134.
(16) Mak, C. H.; Deckert, A. A.; George, S. M. Effects of Coadsorbed Carbon Monoxide on the Surface Diffusion of Hydrogen on Ru(001). *J. Chem. Phys.* **1988**, *89* (8), 5242.
(17) Ciobica, I. M.; Kleyn, A. W.; Van Santen, R. A. Adsorption and Coadsorption of CO and H on Ruthenium Surfaces. *J. Phys. Chem. B* **2003**, *107* (1), 164−172.
(18) Riedmüller, B.; Papageorgopoulos, D. C.; Berenbak, B.; van Santen, R. A.; Kleyn, A. W. Magic" Island Formation of CO Coadsorbed with H on Ru(0001). *Surf. Sci.* **2002**, *515*, 323−336.
(19) Ueta, H.; Groot, I. M. N.; Juurlink, L. B. F.; Kleyn, A. W.; Gleeson, M. A. Evidence of Stable High-Temperature Dx-CO Intermediates on the Ru(0001) Surface. *J. Chem. Phys.* **2012**, *136*, 114710.
(20) Diemant, T.; Rauscher, H.; Bansmann, J.; Behm, R. J. Coadsorption of Hydrogen and CO on Well-Defined Pt35Ru65/Ru(0001) Surface Alloys-Site Specificity vs. Adsorbate-Adsorbate Interactions. *Phys. Chem. Chem. Phys.* **2010**, *12*, 9801.
(21) Hartmann, H.; Bansmann, J.; Diemant, T.; Behm, R. J. Interaction of Coadsorbed CO and Deuterium on a Bimetallic, Pt Monolayer Island Modified Ru(0001) Surface. *J. Phys. Chem. C* **2014**, *118*, 28948.
(22) Chen, Q.; Liu, J.; Zhou, X.; Shang, J.; Zhang, Y.; Shao, X.; Wang, Y.; Li, J.; Chen, W.; Xu, G.; et al. Unveiling Structural Evolution of CO Adsorption on Ru(0001) with High-Resolution STM. *J. Phys. Chem. C* **2015**, *119*, 8626−8633.
(23) RHK Technology, Inc., 1050 East Maple Road, Troy, MI 48083, USA.
(24) Cerdá, J.; Van Hove, M. A.; Sautet, P.; Salmeron, M. Efficient Method for the Simulation of STM Images. I. Generalized Green-Function Formalism. *Phys. Rev. B: Condens. Matter Mater. Phys.* **1997**, *56* (24), 15885−15899.
(25) Soler, J. M.; Artacho, E.; Gale, J. D.; García, A.; Junquera, J.; Ordejón, P.; Sánchez-Portal, D. The SIESTA Method for Ab Initio Order-N Materials. *J. Phys.: Condens. Matter* **2002**, *14*, 2745.
(26) Perdew, J. P.; Burke, K.; Ernzerhof, M. Generalized Gradient Approximation Made Simple. *Phys. Rev. Lett.* **1996**, *77* (18), 3865−3868.
(27) Rossen, E. T. R.; Flipse, C. F. J.; Cerdá, J. I. Lowest Order in Inelastic Tunneling Approximation: Efficient Scheme for Simulation of Inelastic Electron Tunneling Data. *Phys. Rev. B: Condens. Matter Mater. Phys.* **2013**, DOI: 10.1103/PhysRevB.87.235412.
(28) Williams, E. D.; Weinberg, W. H. The Geometric Structure of Carbon Monoxide Chemisorbed on the Ruthenium (001) Surface at Low Temperatures. *Surf. Sci.* **1979**, *82* (1), 93−101.
(29) Maier, S.; Stass, I.; Cerdá, J. I.; Salmeron, M. Bonding of Ammonia and Its Dehydrogenated Fragments on Ru(0001). *J. Phys. Chem. C* **2012**, *116* (48), 25395−25400.
(30) Rose, F.; Tatarkhanov, M.; Fomin, E.; Salmeron, M. Nature of the Dissociation Sites of Hydrogen Molecules on Ru(001). *J. Phys. Chem. C* **2007**, *111* (51), 19052−19057.
(31) Feng, X.; Cerdá, J. I.; Salmeron, M. Orientation-Dependent Interaction between CO_2 Molecules Adsorbed on Ru(0001). *J. Phys. Chem. Lett.* **2015**, *6*, 1780.
(32) Trost, J.; Zambelli, T.; Wintterlin, J.; Ertl, G. Adsorbate-Adsorbate Interactions from Statistical Analysis of STM Images: N/Ru(0001). *Phys. Rev. B: Condens. Matter Mater. Phys.* **1996**, *54* (24), 17850−17857.
(33) Longwitz, S. R.; Schnadt, J.; Vestergaard, E. K.; Vang, R. T.; Lægsgaard, E.; Stensgaard, I.; Brune, H.; Besenbacher, F. High-Coverage Structures of Carbon Monoxide Adsorbed on Pt(111) Studied by High-Pressure Scanning Tunneling Microscopy. *J. Phys. Chem. B* **2004**, *108*, 14497−14502.
(34) Toyoshima, R.; Yoshida, M.; Monya, Y.; Suzuki, K.; Amemiya, K.; Mase, K.; Mun, B. S.; Kondoh, H. A High-Pressure-Induced Dense CO Overlayer on a Pt(111) Surface: A Chemical Analysis Using in Situ near Ambient Pressure XPS. *Phys. Chem. Chem. Phys.* **2014**, *16*, 23564−23567.
(35) Thomas, G. E.; Weinberg, W. H. The Vibrational Spectrum and Adsorption Site of CO on the Ru(001) Surface. *J. Chem. Phys.* **1979**, *70* (3), 1437.
(36) Starr, D. E.; Bluhm, H. CO Adsorption and Dissociation on Ru(0001) at Elevated Pressures. *Surf. Sci.* **2013**, *608*, 241−248.
(37) Jakob, P. High Density Gradients in the $(\sqrt{3}x\sqrt{3})R30°$-CO Layer on Ru(0001). *J. Chem. Phys.* **2004**, *120*, 9286.

DOI: 10.1021/acs.jpcb.7b05657
J. Phys. Chem. B 2018, 122, 649−656